DOI 10.5162/sensoren2019/1.4.3

Concepts for Accurate Electrical Conductivity Measurement of Liquids in Industrial Process Analytics

Michael Vogt[1,2], Santiago Hidalgo[2], Malte Mallach[3], Theresia Lange[3], Jan Förster[3], Thomas Musch[2]
[1]KROHNE Messtechnik GmbH, Ludwig-Krohne-Str. 5, 47058 Duisburg, Germany
[2]Institute of Electronic Circuits, Ruhr University Bochum, 44780 Bochum, Germany
[3]KROHNE Innovation GmbH, Ludwig-Krohne-Str. 5, 47058 Duisburg, Germany

Summary

The electrical conductivity of liquids is of interest in many industrial processes, for example in water desalination, cleaning, mixing of different liquids, analysis of acids and bases, etc. In this contribution, specifically two-electrode conductivity sensors are discussed. A problem with this type of sensor is that a double layer (DL) is given at the interfaces between each of the electrodes and the liquid, resulting in varying and unpredictable diffusion capacitances. For this reason, the electrical resistance of the liquid is not directly accessible from measurements of the sensor input impedance at low frequencies. For accurate determination of the conductivity, the parasitic and disturbing diffusion capacitances, as well as the unknown capacitance of the liquid and the parasitic sensor capacitance have to be eliminated from the measured impedance. The approach in electrical impedance spectroscopy (EIS) is to measure over a very large frequency range for explicitly determining and eliminating the unknown network elements. The motivation behind the work presented here is to allow for precise conductivity measurement at only low frequencies in the range of some kHz. Very advantageously with this, low-cost and low-demanding sensor electronics can be utilized for the realization of according industrial sensors. An equivalent circuit network model of the sensor has been analyzed in detail for this purpose. Approaches for estimating the resistance of the liquid from low frequency measurements of the sensor input impedance are presented and discussed. Finally, the resulting systematic measurement error has been evaluated based on the network model and experimentally.

Keywords: Conductivity measurement, constant phase element, electrical impedance spectroscopy, equivalent circuit, coaxial sensor.

Introduction

Liquids containing dissociated ions, which are referred to as *electrolytes*, have an electrical conductivity that increases with increasing concentration of the ions. Electrical *conductivity sensors* are widely used for easy and continuous in-line monitoring and control of various processes in chemistry, water treatment, and many other applications.

Electrical impedance spectroscopy (EIS) can be understood as an extension of conductivity sensors to additionally also perform measurements of the electrical permittivity and to measure over a much wider frequency range. Numerous works have already been published on using EIS, covering various applications and the analysis of very different substances [1-6].

In this contribution, a model-based approach for eliminating the parasitic network elements from the measured sensor input impedance at relatively *low* frequencies is presented and evaluated. The underlying concept can be understood as an *extrapolation* to measurements at high frequencies, which are in EIS *explicitly* performed. The advantage is that a low-cost digital-to-analog converter (DAC) and analog-to-digital converter (ADC) with a low sampling frequency can be utilized for direct signal generation and digitization, respectively. Accordingly, a microcontroller with low complexity and low power consumption can be used for the sensor electronics and for realizing inexpensive industrial sensors. Low power is very interesting if for example a 4 to 20 mA current loop should be used as field bus interface and also as power supply of the sensor. The available computing power is very limited in this case, so that complicated parameter estimation approaches like the ones used in EIS cannot be implemented.

It will be shown below that the sensor input impedance at low frequencies is dominated by the series connection of the diffusion

capacitances and the resistance of the liquid. On the other hand, the parallel connection of the resistance with the capacitances of the liquid and the sensor dominates at high frequencies. We have defined two characteristic frequency points for a more detailed quantitative analysis of the sensor input impedance in the transition region between the two border cases at medium frequencies.

Electrical Conductivity Sensor

In Fig. 1 a), the setup of a *two-electrode coaxial conductivity sensor* is illustrated, and Fig. 1 b) shows a practical realization of such a sensor.

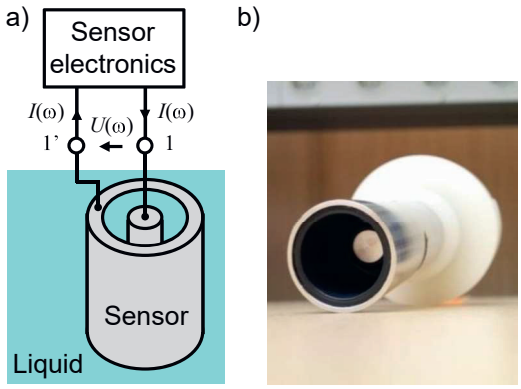

Fig. 1: Two-electrode coaxial electrical conductivity sensor: a) Illustration, b) photo of realized sensor.

This type of sensor is preferably utilized for measurements of liquids with small electrical conductivity. The sensor is directly immersed into the liquid to be analyzed. Using sensor electronics connected to the sensor input port 1/1', see Fig. 1 a), the impedance into the sensor, with the liquid under test between the two electrodes, is measured.
The complex *sensor input impedance* $Z(\omega) = U(\omega) / I(\omega) = R(\omega) + \mathrm{j} \cdot X(\omega)$ over the (angular) frequency ω is derived from the measured voltage $U(\omega)$ across the sensor and the current $I(\omega)$ flowing into the sensor.

Equivalent Circuit Network Model

In Fig. 2, an equivalent circuit network model of the two-electrode conductivity sensor immersed into the liquid is shown.
The *conductance* $G_\mathrm{L} = 1 / R_\mathrm{L} = \sigma_\mathrm{L} / k_\mathrm{cell}$ of the liquid is proportional to its *electrical conductivity* σ_L, with the *resistance* R_L of the liquid and the so-called '*cell constant*' k_cell of the sensor. The latter parameter depends on the geometry (size, distance) of the two electrodes.

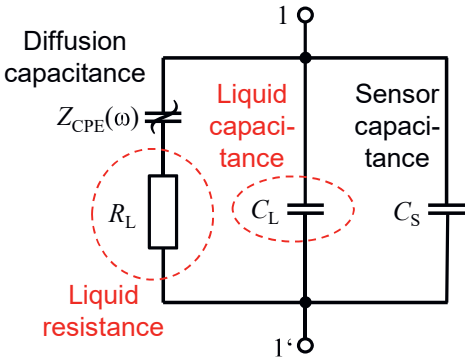

Fig. 2: Equivalent circuit network model: Resistance R_L and capacitance C_L of the liquid, parasitic constant phase element (CPE) $Z_\mathrm{CPE}(\omega)$ (double layers), parasitic sensor capacitance C_S.

At the interfaces between each of the two electrodes and the liquid (being an electrolyte), a *double layer* (DL) builds up. The resulting series connection of these two DLs can be summarized in one network element. A so-called *constant phase element* (CPE) with an impedance $Z_\mathrm{CPE}(\omega)$ described as follows is a good model for the DLs (with $0 < n \leq 1$):

$$Z_\mathrm{CPE}(\omega) = \frac{1}{Q_0 \cdot (\mathrm{j}\omega)^n} = \frac{\cos\left(n \cdot \frac{\pi}{2}\right) - \mathrm{j} \sin\left(n \frac{\pi}{2}\right)}{Q_0 \cdot \omega^n} \qquad (1)$$

The impedance $Z_\mathrm{CPE}(\omega)$ is defined by the two parameters n and Q_0, and it has a *constant phase* over the (angular) frequency ω. For $n = 1$, the CPE is equal to a pure *capacitance* Q_0. In the general case $0 < n < 1$, the CPE is a *lossy* capacitance, whereby the resistance and the reactance of the CPE impedance (having a constant phase) *both* change over frequency, see (1). With the frequency going to infinity, the impedance $Z_\mathrm{CPE}(\omega)$ goes in any case to zero.
The capacitance $C_\mathrm{L} = \varepsilon_\mathrm{L} / k_\mathrm{cell,\varepsilon}$ of the liquid is proportional to its permittivity $\varepsilon_\mathrm{L} = \varepsilon_\mathrm{r,L} \cdot \varepsilon_0$ (relative permittivity $\varepsilon_\mathrm{r,L}$, vacuum permittivity ε_0), with a cell constant $k_\mathrm{cell,\varepsilon}$. In the case of metallic electrodes with no additional dielectric coating etc., $k_\mathrm{cell,\varepsilon} \approx k_\mathrm{cell}$ is given. The parallel capacitance C_S in Fig. 2 summarizes any given additional parasitic input capacitances at the port 1/1' of the sensor. This might include the capacity of the cable connection to the electrodes.

Sensor Input Impedance

In the following, the task of deriving the *electrical conductivity* σ_L of the *liquid* from the measured impedance $Z(\omega)$ data at the port 1/1', see Fig. 2, is discussed:

$$Z(\omega) = \frac{R_L + Z_{CPE}(\omega)}{1 + j\omega \cdot (C_L + C_S) \cdot (R_L + Z_{CPE}(\omega))} \qquad (2)$$

The resistance R_L is not directly accessible from this measurement. Accordingly, the challenge is to eliminate the unknown parallel capacitance $C_L + C_S$ of the liquid and the sensor, and also the CPE impedance $Z_{CPE}(\omega)$ from the measurement. The *parasitic* CPE is very unpredictable and unknown, and it can largely vary over time and over different samples of the same type of sensor. The CPE parameters n and Q_0, see (1), depend largely on various properties (electrodes material, surface roughness, and surface area of the electrodes, type and conductivity of the liquid, etc.).

In principle, the sensor input impedance $Z(\omega)$ also gives access to the *electrical permittivity* ε_L of the liquid, as long as C_L can be separated from C_S in the parallel connection, see Fig. 2. In *industrial* applications, however, the electrical *conductivity* σ of the liquid is the primarily interesting parameter to be measured. Taking the measured temperature into account, the *concentration of dissolved ions* in the liquid can be derived from the measured conductivity.

In the general case, the permittivity of the liquid is unknown and might largely vary (e.g. $\varepsilon_{r,L} = 2.3$ for gasoline, $\varepsilon_{r,L} = 80$ for water). For this reason, the liquid's capacitance C_L has been explicitly taken into consideration in Fig. 2 as an unknown *parasitic* network element. Accordingly, C_L has to be eliminated from the measured $Z(\omega)$. The same applies for the sensor capacitance C_S, although it might be largely compensated by a *calibration* of the sensor. Despite of this, a possibly remaining residual capacitance after calibration is also explicitly taken into account by means of C_S.

Characteristic Frequency Points

In EIS, parametric *Nyquist plots* of the (conjugate-complex) sensor input impedance $Z^*(\omega) = R(\omega) - j\,X(\omega)$ over frequency are quite commonly used to visualize measurement results etc. [2-5]. Nyquist plots are also used in the following to discuss strategies for deriving the resistance R_L of the liquid from $Z(\omega)$ in more detail. The plots also give an easy understanding and access to given systematic measurement errors.

In Fig. 3, a *normalized* Nyquist plot of $Z^*(\omega)/R_L$ is illustrated (under some limitations and for varying parameter n).

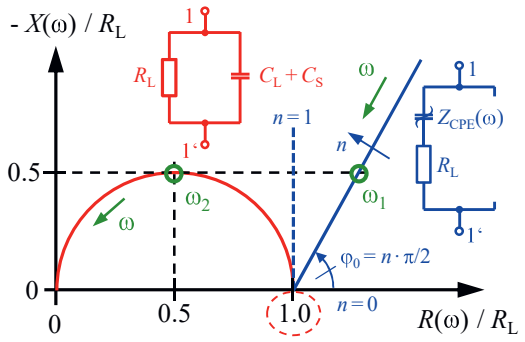

Fig. 3: Nyquist plot (illustration): Conjugate-complex normalized sensor input impedance $Z^*(\omega)/R_L$ for border cases of solely series and parallel connections of parasitic elements with the resistance R_L of the liquid; definition of characteristic frequency points ω_1 and ω_2.

The *blue* curve in Fig. 3 shows the *border case* of *negligibly small* liquid and sensor capacitances (i.e. $C_S = C_L = 0$). Under this condition, a *linear* function over the (angular) frequency ω is given, see (1). The slope of the according curve depends on the CPE parameter n (see the angle $\varphi_0 = n \cdot \pi/2$ in Fig. 3).

Because the reactive current through C_S and C_L, see Fig. 2, only plays a significant role at *higher* frequencies, the blue plot is a good approximation of the sensor input impedance at (relatively) *low* frequencies. A similar consideration can be made for the *border case* of having a *negligibly small* CPE impedance (i.e. for $Z_{CPE}(\omega) = 0$) at (relatively) *high* frequencies. In this case, a half-circular curve is given in the Nyquist plot, see the *red* curve in Fig. 3. This follows from calculating the reciprocal (*Möbius transformation*) of the sensor input *admittance* $Y(\omega)$ in this case. The latter has a constant real part and an imaginary part proportional to the frequency as follows, see (2) with $Z_{CPE}(\omega) = 0$:

$$Y(\omega) = \frac{1}{Z(\omega)} = R_L^{-1} + j\,\omega \cdot (C_L + C_S) \qquad (3)$$

Obviously, for the general case of the sensor according to Fig. 2, the CPE and the two parallel capacitances *all* have to be taken into account at the same time. Especially at *medium* frequencies, a Nyquist plot *in-between* the blue and the red curves in Fig. 3 is expected. However, at *low* and *high* frequencies, the two border cases discussed above will still be a good approximation. For testing the validity of this assumption, we have defined the two *characteristic frequency points*

ω_1 and ω_2 as shown in Fig. 3. Using (1) and (3), they are given as follows:

$$\omega_1 = \left(\frac{2\cdot\sin(n\cdot\pi/2)}{R_L\cdot Q_0}\right)^{1/n}, \quad \omega_2 = \frac{1}{R_L\cdot(C_L+C_S)} \qquad (4)$$

The blue and red curves in Fig. 3 will only be good approximations in the case that $\omega_2 >> \omega_1$ is given. For a more detailed analysis, the *ratio* $\omega_{rel} = \omega_2 / \omega_1$ of the two characteristic frequency points is used below as an important parameter:

$$\omega_{rel} = \frac{\omega_2}{\omega_1} = \frac{R_L^{\left(\frac{1}{n}-1\right)}}{(C_L+C_S)} \cdot \left(\frac{Q_0}{2\cdot\sin(n\cdot\pi/2)}\right)^{1/n} \qquad (5)$$

As given in (5), the Nyquist plot at *medium* frequencies depends on the given *relationship* between the parasitic elements Q_0, n, C_L+C_S, and relative to R_L.

Numerical Simulations

The detailed sensor input impedance over a large frequency range has been analyzed based on numerical simulations using the complete equivalent circuit network model in Fig. 2. Using (1), (4), and (5), the normalized sensor input impedance according to (2) can be expressed as follows with the *normalized frequency* $\omega_n = \omega / \omega_1$:

$$\frac{Z(\omega)}{R_L} = \frac{1+\frac{1}{2\cdot\sin(n\cdot\pi/2)\cdot(j\omega_n)^n}}{1+j\omega_n/\omega_{rel}\cdot\left(1+\frac{1}{2\cdot\sin(n\cdot\pi/2)\cdot(j\omega_n)^n}\right)} \qquad (6)$$

The parasitic network elements in (6) are now completely described by ω_{rel} and the CPE parameter n.

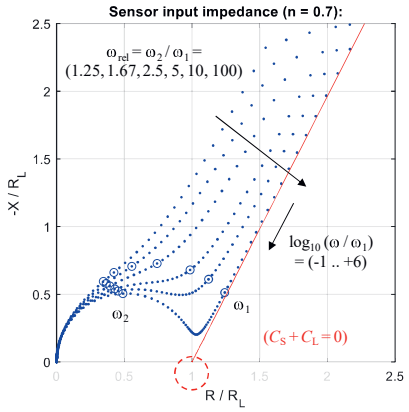

Fig. 4: Nyquist plot: Calculated normalized sensor input impedance $Z^*(\omega)/R_L$ over normalized frequency $\omega_n = \omega/\omega_1$ for parameterization with $n = 0.7$ and varying ratio $\omega_{rel} = \omega_2/\omega_1$ of the characteristic frequencies ω_1 and ω_2.

As an example, the blue dots in Fig. 4 show the Nyquist curves of the calculated normalized sensor input impedance according to (6) for $n = 0.7$ and for varying $\omega_{rel} = \omega_2/\omega_1$ (in the range from 1.25 to 100) at discrete (exponentially increasing) normalized frequencies $\omega_n = \omega/\omega_1$ (in the range from 10^{-1} to 10^6). As expected and discussed above, the linear and circular curves in Fig. (3) are only good approximations for a large ratio of the two characteristic frequency points.

Based on the results in Fig. 4 the resulting *systematic measurement error* in case of using one of the two approximations can be analyzed. The red curve is the sensor input impedance for the low-frequency approximation with $C_S = C_L = 0$. The blue circles in Fig. 4 indicate the characteristic frequency points ω_1 and ω_2 in each of the Nyquist plots. This allows for choosing reasonable measurement frequencies for a sufficiently small measurement error in the case of using the approximations.

Fig. 5 shows another example of the calculated normalized sensor input impedance for $n = 0.3$.

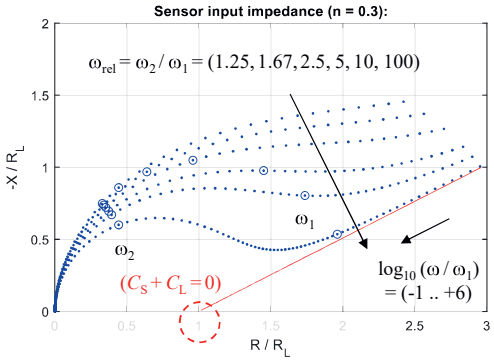

Fig. 5: Nyquist plot: Calculated normalized sensor input impedance for $n = 0.3$.

It can be seen that the relative deviations from the approximations are now (for $n = 0.3$) much larger as compared to the example in Fig. 4 (with $n = 0.7$). Consequently, the actually given parameters n and ω_{rel}, describing the parasitic elements, have a significant effect.

Measurement Concepts

The usual approach in EIS is to measure the sensor input impedance over a very *large frequency range* and to explicitly determine the parameters of an equivalent circuit network model. This is done by fitting the parametric network model to the *wideband* measurement data [1].

It has already been discussed above that our goal is to only utilize measurements at *low* frequencies for estimating the resistance R_L of the liquid. Accordingly, we aim at using the

border case and approximation given by neglecting the liquid and sensor capacitances ($C_S = C_L = 0$) discussed above, see the blue curve in Fig. 3.
A first concept is to use the measured impedances at only *two* low *measurement frequencies* for estimating R_L. Referring to the red curves in Figs. 4 and 5, this can be understood as a *linear extrapolation* from these two points to the intersection with the abscissa in the Nyquist plot, see Fig. 6 a).

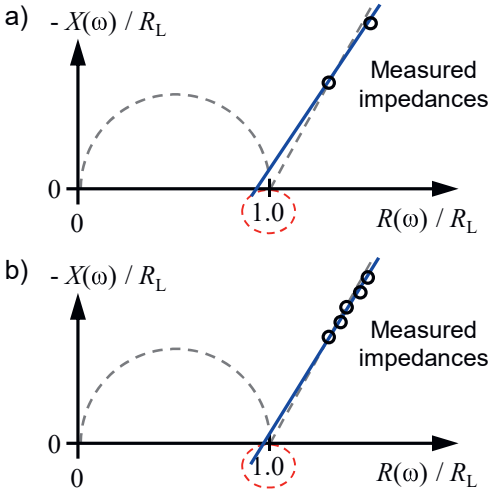

Fig. 6: Nyquist plot (illustration): a) Linear extrapolation using impedance measurements at only two low measurement frequencies, b) linear regression fit using multiple measurement frequencies; the same frequency interval is covered with both concepts in this example.

The characteristic frequency points ω_1 and ω_2 in (4) allow to assess the applicability of this approach in more detail. First, $\omega_2 >> \omega_1$ (i.e. $\omega_{rel} >> 1$) should be fulfilled so that the linear case is a sufficiently good approximation at low frequencies for the actually given situation, see Figs. 4 and 5. Second, the utilized measurement frequencies should be much smaller than ω_1. This criterion is to guarantee that the measurements are actually done in the linear part of the curve. Accordingly, *systematic* measurement errors given by applying the linear approximation are minimized. As a further criterion, the distance between the two frequency points should be as large as possible. The goal behind this is to be as less sensitive as possible against *random* measurement errors (given by the noise of the sensor electronics). However, the linear approximation has of course still to be valid at the lower frequency.
A reasonable second concept is to extend the linear extrapolation to impedance measurements at *multiple* low frequencies by using a *linear regression fit*, see Fig. 6 b). The interval of utilized frequencies should of course comply with the same criteria formulated for the first approach.

Experimental Evaluation

The findings and approaches discussed above have also been evaluated by means of experimental measurements. The coaxial conductivity sensor shown in Fig. 7 a) (see also Fig. 1 b), stainless steel electrodes, cell constant $k_{cell} = 1.0\ \mathrm{cm}^{-1}$) has been used for all measurements.

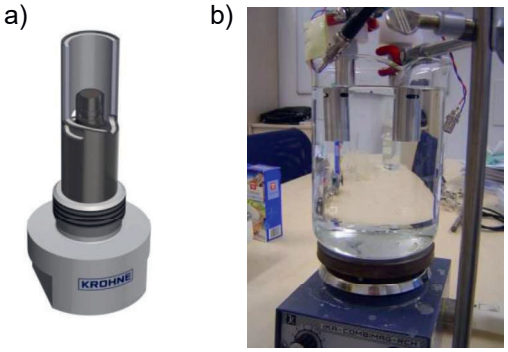

Fig. 7: a) Coaxial measurement sensor (CAD-model), b) realized measurement setup with a magnetic stirrer.

A *vector network analyzer* (VNA, model Bode 100; OMICRON electronics GmbH, Klaus, Austria) has been utilized for measuring the complex sensor input impedance. The VNA has been connected to the sensor using a coaxial cable ($Z_L = 50\,\Omega$ line impedance). Prior to the measurements, the VNA was calibrated at the sensor port using a *TOSM* (through, open, short, $50\,\Omega$ match) *calibration* scheme.
Salt-water with varying salinity (0 to $100\,\mathrm{g/l}$ of NaCl) has been tested. A magnetic stirrer was used to guarantee for a good dissolution of the salt, see Fig. 7 b). The advantage of using *water* (with its very large relative permittivity $\varepsilon_{r,L} \approx 80$) is, that the *worst-case* with regard to introducing disturbances to the conductivity measurement by the capacitance C_L of the liquid is analyzed.

Measurement Results

In Fig. 8, Nyquist plots of the measured (absolute) sensor input impedance $Z(\omega)$ over a large frequency range from $10\,\mathrm{Hz}$ to $150\,\mathrm{kHz}$ are shown for varying salinity.
It can be seen that the CPE model (with a constant phase of the impedance over frequency) discussed above fits well to the measured impedance. Additionally, in the blue curve (tap water with no salt added at all), the

expected influence of the parallel capacitances (liquid and sensor) can clearly be seen.

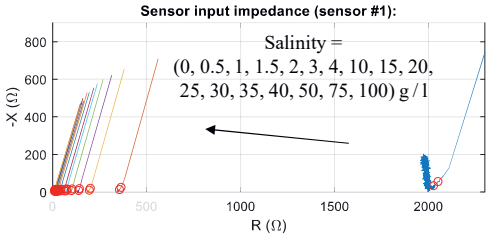

Fig. 8: Nyquist plots: Measured sensor input impedance $Z^*(\omega)$ (sensor #1) over a large frequency range ($10\,\mathrm{Hz}$ to $150\,\mathrm{kHz}$) for varying salinity, measurements at $1\,\mathrm{kHz}$ and $3\,\mathrm{kHz}$ marked with red circles.

With increasing salinity (i.e. with increasing conductivity and decreasing resistance of the liquid), however, no large influence of the capacitances can be identified any more.

In order to estimate the *actually given* ('true') resistance R_L of the liquid for each different salinity, we have used the complex sensor input admittance $Y(\omega) = 1/Z(\omega)$ at the *highest* measurement frequency of $150\,\mathrm{kHz}$. The underlying assumption is that the impedance $Z_\mathrm{CPE}(\omega)$ of the CPE at this high frequency is negligibly small against R_L. According to (3), R_L has been estimated as the inverse of the *real part* of the admittance at that frequency. For the given salinities in the range from 0 to $100\,\mathrm{g/l}$, the accordingly determined R_L is in the range from about $2\,\mathrm{k\Omega}$ down to $8\,\Omega$. Using the nominal cell constant $k_\mathrm{cell} = 1.0\,\mathrm{cm^{-1}}$ of the utilized sensor (which has been optimized by means of electrostatic field simulations), the corresponding conductivity σ is in the range from about $0.5\,\mathrm{mS/cm}$ to $125\,\mathrm{mS/cm}$.

Fig. 8 shows the results obtained with a *first sample* sensor #1 of the utilized sensor type. The same measurements have also been performed using a second sample sensor #2 of the same sensor type. As can be seen in Fig. 7 b), the experiments with the two sensors have been made parallel to each other under exactly the same conditions. The motivation behind this was to investigate deviations from one sample to another in more detail, especially deviations of the CPEs.

In Fig. 9, the Nyquist plots for sensor#2 are shown. The actually given R_L has again been estimated for each varying salinity as described before using the measured impedance at the highest frequency of $150\,\mathrm{kHz}$. The estimates obtained from the measurements with the two sensors #1 and #2 are in a good agreement with each other (maximum deviation smaller $\pm 1.5\%$).

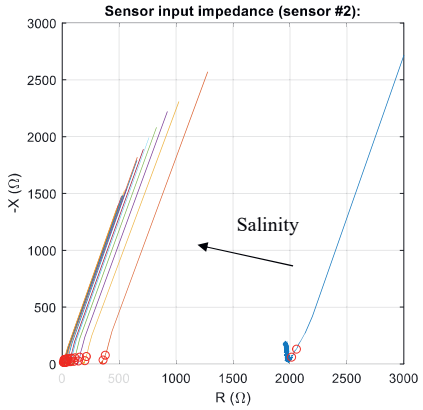

Fig. 9: Nyquist plots: Measured sensor input impedance $Z^*(\omega)$ (sensor #2).

Taking the different scaling of the axes in Figs. 8 and 9 into account, it can be seen that the reactance of the CPE of sensor #2 is much larger as compared to sensor #1 (at the same measurement frequencies). It can be concluded from this that the DL diffusion capacitance (and so the CPE parameter Q_0) is much smaller for sensor #2 compared to sensor #1. A reasonable explanation behind this could be that the two sensors have been used with different intensities and different types of liquids prior to the experiments described here. Accordingly, it is possible that different microscopic surface structures and deposits have been given at the electrodes of the sensors, thus changing the properties of the DLs of each sensor.

For a more detailed analysis, the *normalized* sensor input impedance $Z^*(\omega)/R_\mathrm{L}$ has been calculated (normalized to the estimates for the actually given R_L as discussed above) for each varying salinity and for each of the two sensors.

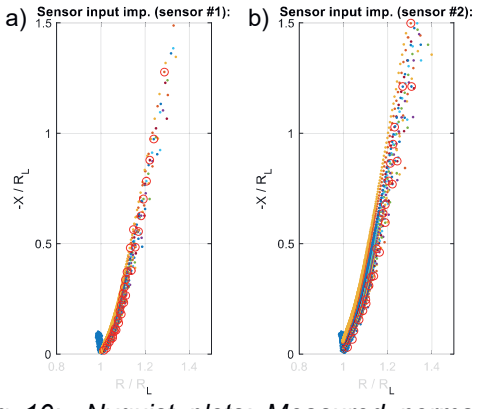

Fig. 10: Nyquist plots: Measured normalized sensor input impedance $Z^*(\omega)/R_\mathrm{L}$ over a large frequency range ($10\,\mathrm{Hz}$ to $150\,\mathrm{kHz}$), measurements at $1\,\mathrm{kHz}$ and $3\,\mathrm{kHz}$ marked with red circles: a) Sensor #1, b) sensor #2.

In Fig. 10, the normalized impedances at the individual frequencies (960 equally spaced measurement frequency points) have been plotted by using *dots*. (For a better visualization, the corresponding consecutive points have been connected with each other by using a *line* in the plots in Fig. 9.) In Figs. 8 and 9, the same colors have been used for each same salinity, and the red circles in Figs. 8 to 10 indicate the two measurement frequencies of $1\,\mathrm{kHz}$ and $3\,\mathrm{kHz}$ for each individual curve.

The variations of the slopes of the curves for each individual sensor #1 and #2 in Figs. 10 a) and b), as well as the variation between the two sensors are very small. This shows that the CPE parameter n remains largely constant over all measurements. It can be seen now the definition of the characteristic frequency point ω_1 in (4) was very reasonable. As discussed above, the CPE parameter Q_0 is smaller for sensor #2 compared to #1. Accordingly, ω_1 is larger for sensor #2 and the normalized impedances with this sensor are more far away from the abscissa as compared to sensor #1 (at the same measurement frequencies). This can be seen very clearly from comparing the positions of the red circles in Figs. 10 a) and b), respectively.

Using this measurement data, both, the *two measurement frequencies* concept as well as the *multiple measurement frequencies* concept discussed above, have been evaluated. As the parallel capacitances play no significant role here (except for the smallest salinity), relatively high measurement frequencies of $1\,\mathrm{kHz}$ and $3\,\mathrm{kHz}$ have been used for the first concept. The second concept has been tested by using 14 equally spaced frequencies in a corresponding interval from $1\,\mathrm{kHz}$ to $3\,\mathrm{kHz}$.

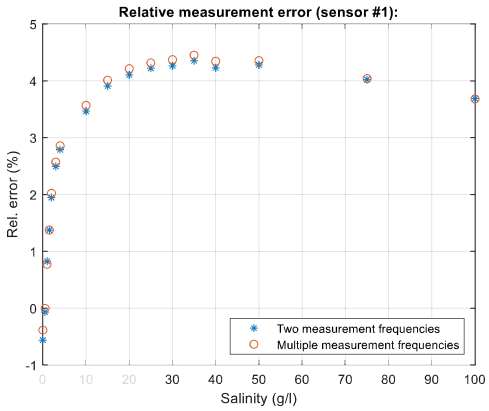

Fig. 11: Relative conductivity measurement errors for varying salinity (sensor #1): Two measurement frequencies and multiple frequencies concepts.

In Fig. 11, the resulting relative measurement errors for the data of sensor #1 are shown (errors referring to the estimated actually given R_L in each case, as described above). It can be seen that, although only measurements at very low frequencies are utilized, the relative measurement error (referring to measurements at a very high frequency of $150\,\mathrm{kHz}$) are quite small. The given errors are smaller than $4.3\,\%$, what is acceptably small. The systematic measurement errors at small salinities (i.e. for small conductivities of the liquid) are even much smaller. The latter is a plausible result, because it confirms again that the CPE is getting less relevant with increasing resistance R_L. The comparison of the errors in Fig. 11 obtained with the two measurement concepts shows no significant difference. Based on the expectation that the second concept, i.e. using a linear regression fit, is less sensitive against electronic noise, it can be concluded that the given signal-to-noise ratio (SNR) with the VNA was sufficiently large and was not a limiting factor here. The deviations given in Fig. 11 are for this reason mainly systematic measurement errors, which are introduced by using the linear approximation.

In Fig. 12, the corresponding measurement errors obtained by using sensor #2 are shown.

Fig. 12: Relative conductivity measurement errors for varying salinity (sensor #2).

Again, the systematic measurement error at small salinities is very low, and an only slightly larger maximum error of $4.9\,\%$ is given. With sensor #2, the errors at larger salinities are much smaller as compared to sensor #1, see Figs. 11 and 12. It is known from (4) that ω_1 generally increases with decreasing R_L (i.e. with increasing salinity) and also with decreasing CPE parameter Q_0. A plausible explanation for the finding here now is that the *increase* of ω_1 *with increasing salinity* is larger for sensor #2, because of its larger Q_0, as compared to sensor #1. Finally, the larger the characteristic frequency ω_1 is, the better the assumption of *linear* curves is actually valid (for the same given low frequencies), see Figs. 4 and 5.

Summary and Conclusions

In this contribution, the applicability of estimating the electrical conductivity of liquids by using measurements of the sensor input impedance at only low frequencies has been analyzed and validated. The motivation behind this was to allow for direct signal generation and digitization using inexpensive and low-complex sensor electronics. This is in some contradiction to the usual approach in EIS of using measurements over a large frequency range for explicitly estimating both, the interesting network elements as well as the parasitic ones.

An equivalent circuit network model of the sensor has been discussed, wherein the DL at the electrodes is modeled as a CPE. The problem with this element is that its properties can largely vary from one sample of the same type of sensor to another. Numerical simulations with the network model have been performed. The goal in this context was to analyze systematic measurement errors, which are introduced by using border case approximations for describing the network model. Accordingly, the applicability of using measurements at low frequencies only has been evaluated. Two different measurement concepts have been investigated. The first approach uses the impedances at only two measurement frequencies for linear extrapolation. In the second concept, linear regression is performed with the measured impedances at multiple discrete frequencies.

Finally, experimental measurements have been performed with salt-water of varying salinity. The presented results show that the systematic measurement, which is introduced by measuring at only small frequencies in the range from $1\,\mathrm{kHz}$ to $3\,\mathrm{kHz}$, is acceptably small.

References

[1] O. Kanoun, U. Tröltzsch: Application of Parameter Extraction Techniques for Impedance Spectroscopy. Instrumentation and Measurement Conf., 2281-2286 (2005); doi: 10.1109/IMTC.2005.1604583

[2] U. Tröltzsch, R. Gruder, O. Kanoun, A. Buchholz, V. Beck: Anwendungspotenziale der Impedanzspektroskopie für die Waschlaugensensorik. GMA/ITG-Fachtagung Sensoren und Messsysteme, 650-661 (2012); doi: 10.5162/sensoren2012/6.2.4

[3] R. Gruder, O. Kanoun: Water Quality Assessment by Combining Impedance Spectroscopy Measurement with Cyclic Voltammetry. AMA Conf. – Sensors, Opto and IRS2, 164-169 (2013); doi: 10.5162/sensor2013/A8.1

[4] A. Abdelkafi, P. Büschel, A. Fendri, O. Kanoun: Impedance Investigation of Milk Dilution. AMA Conf. – Sensors and IRS2, 156-159 (2015); doi: 10.5162/sensor2015/A7.2

[5] A. Fendri, P. Büschel, A. Abelkafi, O. Kanoun, A. Buchholz: AdBlue Quality Control using Impedance Spectroscopy. AMA Conf. – Sensors and IRS2, 830-832 (2015); doi: 10.5162/sensor2015/P7.3

[6] A. Fendri, H. Ghariani, O. Kanoun: Dielectric Spectroscopy for Assessment of Water Content in Edible Oils. Int. Multi-Conf. on Systems, Signals & Devices, 728-732 (2017); doi: 10.1109/SSD.2017.8167027